Electronic Supplementary Information

A Narrowband Red-Emitting Asymmetric Iridium(III) Complex Featuring B- and N-Embedded π-Conjugation Units: Structure, Photophysics and OLED Application

Meng Wu,[1] Nengquan Li,[2] Chao Shi,[1]* Jialiang Song,[1] Ruoqi Zeng,[1] Feiyang Li,[1] Qiuxia Li,[1]* Aihua Yuan[1] and Chuluo Yang[2]*

[1] School of Environmental and Chemical Engineering, Jiangsu University of Science and Technology, Zhenjiang 212003, P. R. China.

[2] College of Materials Science and Engineering, Shenzhen University, Shenzhen 518060, P. R. China.

Corresponding Authors' E-mail address

* shichao@just.edu.cn

* liqiuxia2019@just.edu.cn

* clyang@szu.edu.cn

Contents:

General information

Unless noted, all reagents or solvents were obtained from commercial suppliers and used without further purification. All air sensitive experiments were performed in N_2 atmosphere through schlenk technology. The ligands **L1** and **L2** were synthesized according to literature procesures[1]. The ^1H NMR and ^{13}C NMR spectra were measured by using a Bruker 400 MHz spectrometer at room temperature. Mass spectra was conducted at Thermo QE Orbitrap HDMS. An Edinburgh FS5 spectrofluorometer was used to measure phosphorescence spectral (the slit is set to 2 nm). An Edinburgh FLS-980 spectrometer was used to determine phosphorescence quantum efficiency and lifetimes of the molecule. The PS films (1 wt%) of all the iridium complexes are made by evaporating their CH_2Cl_2 solution in a round-bottomed glass vial. The experiments for cyclic voltametric were performed by using three electrode cell assemblies from an IM6ex instrument (Zahner). A one-compartment cell equipped with a platinum wire counter electrode, a Ag/Ag^+ reference electrode, and a glassy-carbon working electrode was used for all measurements with a scan rate of 100 mVs^{-1}. The concentration of tetrabutylammonium hexafluorophosphate (Bu_4NPF_6) in dichloromethane solution a was 0.10 $molL^{-1}$ and used as supporting electrolyte.

Synthesis and characterization

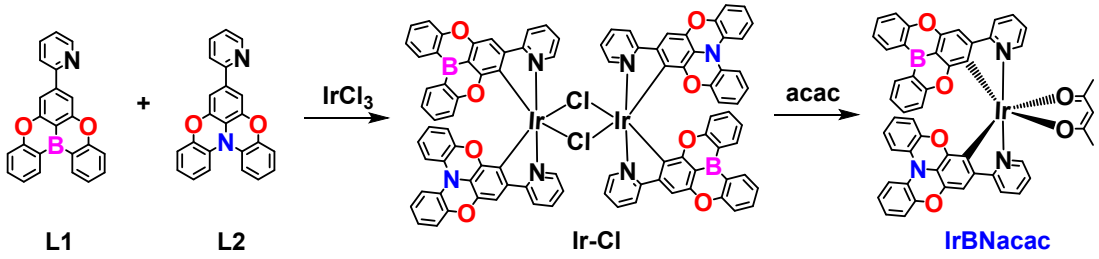

Figure S1. The synthetic routes for the asymmetric heteroleptic iridium complex **IrBNacac**.

IrBNacac: L-2 (0.042 g, 0.12 mmol), L-1 (0.041 g, 0.12 mmol) and $IrCl_3$ (0.035 g, 0.1 mmol) were charged to a 100 mL double-neck reaction bottle, followed by mixture of 2-ethoxyethanol (9 mL) and H_2O (3 mL). The mixture was heated to 110 ^oC for 24 h under N_2. Water (100 mL) was added and the resulting precipitate was filtered. The product has been washed three times with water and dried to give chloro-bridged dimer complex Ir-Cl without further purification. The chloro-bridged dimer complex Ir-Cl (0.185 g, 0.1 mmol), acetylacetone (0.05 mL, 0.5 mmol) and Na_2CO_3 (0.053 g, 0.5 mmol) were charged

to a 100 mL schlenck tube, followed by 2-ethoxyethanol (10 mL). The mixture was heated to 60 °C for 24 h under N_2. The resulting solution was saturated with water and extracted with CH_2Cl_2 three times. The combined organic phase was dried and concentrated in vacuum, and target product was purified by column chromatography on silica gel with CH_2Cl_2/ petroleum ether 3:2 (v/v) to afford red solid. 59 mg (30 %). ^{1}H NMR (400 MHz, CD_2Cl_2) δ 8.56 (m, 2H), 8.50 (m, 2H), 8.22 (d, J = 7.9 Hz, 1H), 7.97 (t, J = 7.1 Hz, 2H), 7.75 (s, 1H), 7.64 (m, 1H), 7.46 (m, 1H), 7.38 (m, 2H), 7.26 (m, 3H), 7.16 (m, 2H), 6.85 (m, 8H), 5.79 (d, J = 8.4 Hz, 1H), 5.29 (s, 1H), 1.79 (s, 3H), 1.73 (s, 3H). ^{13}C NMR (101 MHz, CD_2Cl_2) δ 185.22, 185.16, 169.01, 161.81, 161.14, 153.47, 149.66, 149.40, 148.01, 137.68, 137.36, 135.18, 134.60, 133.73, 133.43, 123.59, 123.40, 122.95, 122.55, 122.24, 121.21, 120.40, 119.53, 119.05, 118.45, 117.41, 117.12, 115.29, 114.78, 107.95, 104.53, 101.03, 28.88, 28.79. $C_{51}H_{33}BIrN_3O_6$ calcd: C, 62.07; N, 4.26; H, 3.37. Found: C, 62.04; N, 4.23; H, 3.39. HR-MS: m/z calcd for $C_{51}H_{33}BIrN_3O_6$ $[M+H]^+$: 988.2092. Found: 988.2170.

X-ray crystal structure analysis

The single-crystal of **IrBNacac** was obtained by slow diffusion of ethanol to its CH_2Cl_2 solution, respectively. The X-ray diffraction data were collected on a Bruker Smart CCD Apex DUO diffractometer with graphite monochromated Mo Kα radiation (λ = 0.71073 Å) using the ω-2θ scan mode. All crystal datas are deposited in The Cambridge Crystallographic Data Centre (CCDC: 2209564 for **IrBNacac**).

Table S1. Crystallographic data for **IrBNacac**.

Complex	IrBNacac
chemical formula	$2(C_{51}H_{33}IrBN_3O_6)$, $3(CH_2Cl_2)$
formula weight	2228.40
crystal size (mm)	0.08 × 0.10 × 0.11
temperature (K)	150
radiation	0.71073
crystal system	Triclinic
space group	P-1
a(Å)	12.8234(6)
b(Å)	13.7765(6)

c(Å)	15.0704(7)
α(°)	62.941(2)
β(°)	83.140(2)
γ(°)	69.284(2)
V(Å^3)	2214.89(18)
Z	1
ρ($_{calc}$) (g/cm^3)	1.671
F (000)	1106
absorp.coeff. (mm^{-1})	3.253
θ range (deg)	2.0 to 25.0
reflns collected	41809 (R_{int} = 0.089)
indep. reflns	7774
Refns obs.[$I>2\sigma(I)$]	6654
data/restr/paras	7774/0/630
GOF	1.07
R_1/wR_2 [$I>2\sigma(I)$]	0.0456/0.1169
R_1/wR_2 (all data)	0.0551/0.1258
larg peak and hole(e/Å^3)	1.35/–0.90

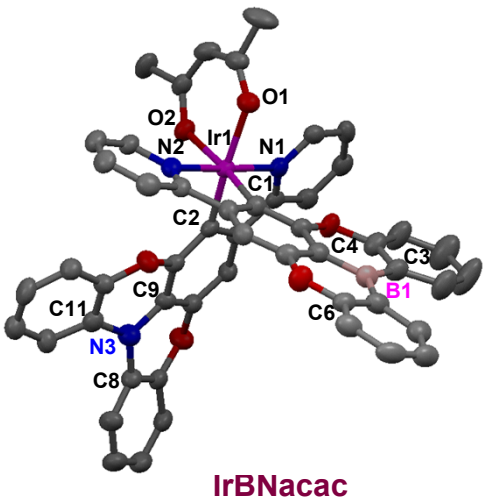

IrBNacac

Figure S2. The single crystal structure of **IrBNacac**, the hydrogen atoms have been omitted for clarity, selected bond lengths (Å) and angles (°): Ir1−C1: 2.018(7), Ir1−C2: 1.996(8), Ir1−N1: 2.038(7), Ir1−N2: 2.051(7), Ir1−O1: 2.123(5), Ir1−O2: 2.124(6), N3−C11: 1.421(12), N3−C9: 1.423(12), N3−C8: 1.411(11), B1−C6: 1.530(13), B1−C4: 1.507(14), B1−C3: 1.546(14); C1–Ir1–N2: 79.4(3), C2–Ir1–N1:

80.2(3), O1–Ir1–O2: 89.3(2), C1–Ir1–O1: 172.2(3), C2–Ir1–O2: 172.0(3), N1–Ir1–N2: 178.1(3), C8–N3–C11: 126.9(8), C3–B1–C6: 131.6(9).

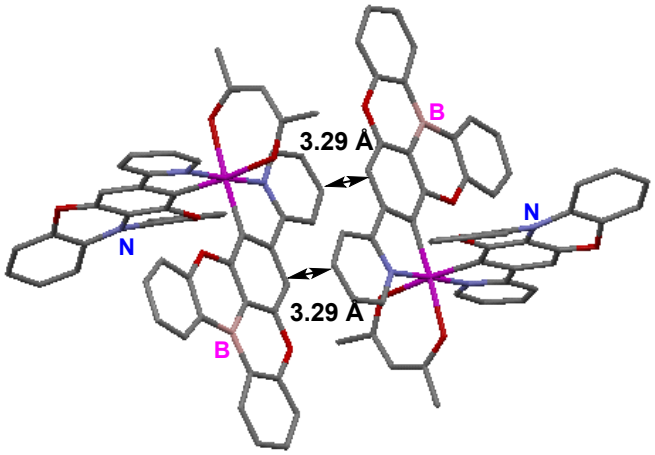

π-π stacking mode 3

Figure S3. The intermolecular interaction of the complex **IrBNacac** in crystal state.

Photophysical properties

Table S2 UV−vis absorption data of **IrBNacac** in dichloromethane at 298 K.

Complex	λ_{abs} nm (log ε)
IrBNacac	232(4.33), 261(4.35), 329(4.04), 365(3.72), 419(3.66), 530(2.90)

Measured in dichloromethane at a concentration of 2.25×10^{-5} M, and log ε values are shown in parentheses at room temperature.

Table S3 Photophysical properties of **IrBNacac** at 298 K.

Complex	PL[a]/[b] (nm)	$E_{1/2}^{Ox}$ (eV)	E_g[c] (eV)	HOMO/LUMO[c] (eV)	Φ_{PL}[b] (%)	τ[b] (ns)
IrBNacac	625/623	0.11/0.29/0.48	2.21	-4.91/-2.70	35 %	6227

[a] Recorded in dichloromethane (2.55×10^{-5} M) at 298 K with an excitation wavelength of 370 nm. Φ_p is referred to absolute quantum yields of phosphorescence determined by employing an integrating sphere. [b] recorded in PS films (1 wt%) (excitation wavelength 370 nm). [c] The HOMO(eV) = $-(E_{onset}^{ox} + 4.8)$eV, Eg = 1240/λ, λ is absorption wavelength threshold. LUMO(eV) = Eg + HOMO

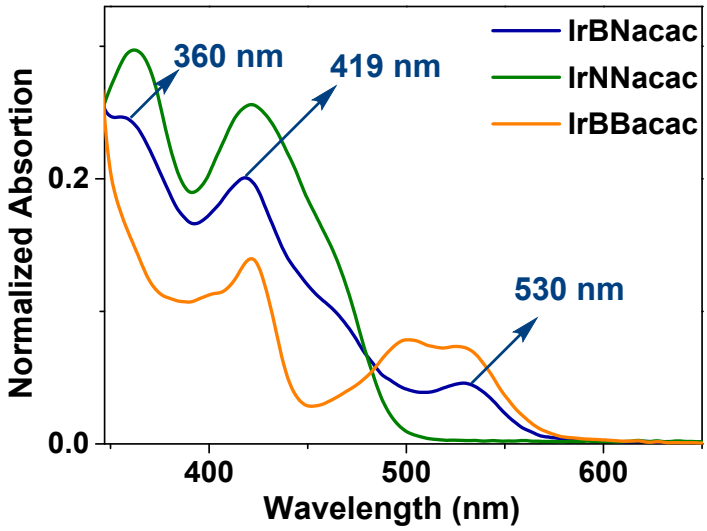

Figure S4. Absorption spectra of the iridium complex **IrBNacac** and model iridium complexes (**IrBBacac** and **IrNNacac**) in CH_2Cl_2 solution。

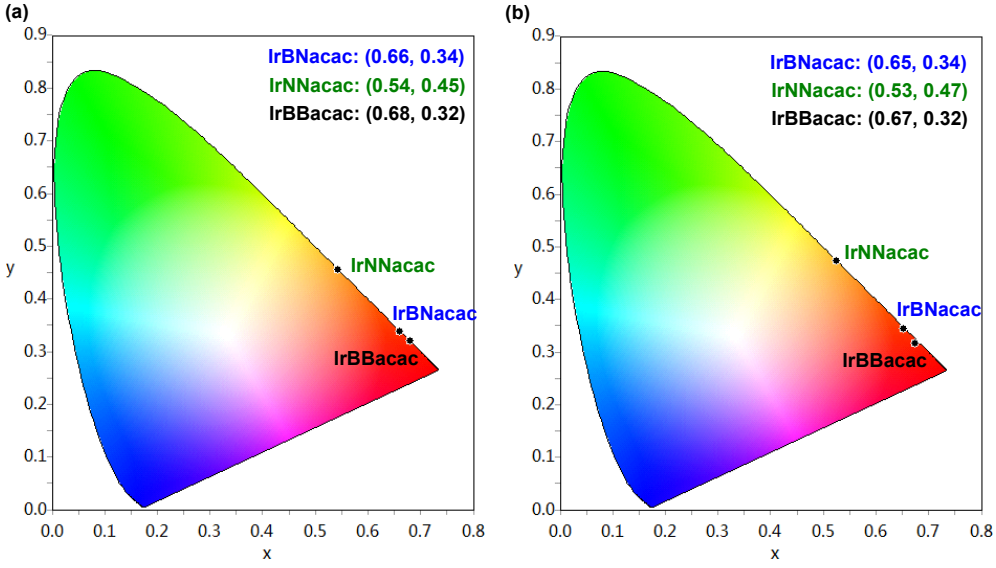

Figure S5. The CIE coordinates of photoluminescence spectra of iridium complexes (**IrBNacac**, **IrNNacac** and **IrBBacac**) in (a) dichloromethane solution and (b) PS (1 wt%) films.

(a)

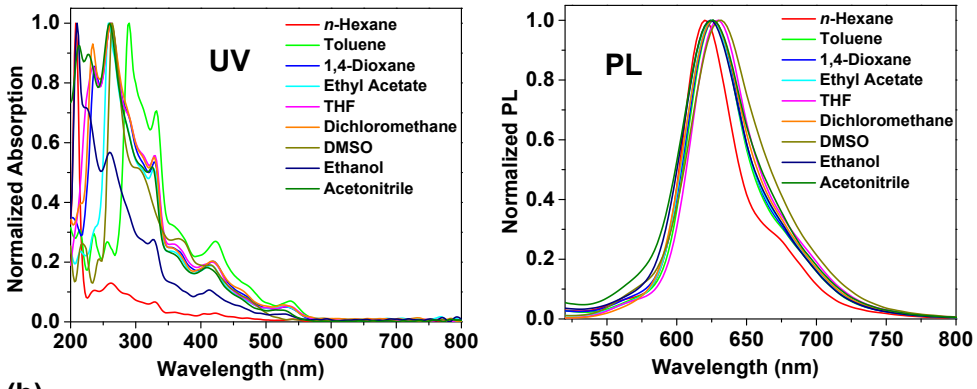

(b)

	$f(\varepsilon,n)$	$\nu_a-\nu_f/cm^{-1}$
n-Hexane	0.0012	2355.2561
Toluene	0.014	2647.53303
1,4-Dioxane	0.021	2893.48363
Ethyl Acetate	0.2	2964.95304
THF	0.21	2853.57589
Dichloromethane	0.217	3000.89117
DMSO	0.264	2695.73371
Ethanol	0.289	2913.75291
Acetonitrile	0.305	3073.17815

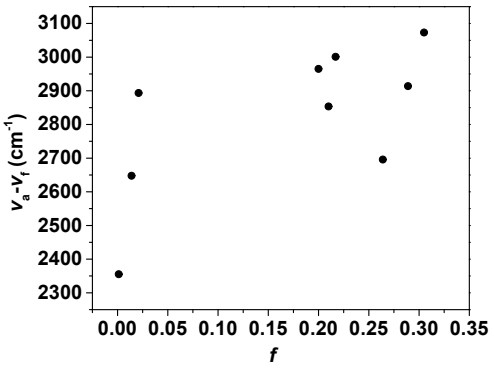

Figure S6. (a) The UV-Vis and PL spectrum of the iridium complex **IrBNacac** in different solutions. (b) Mataga–Lippert plots for CT emission of iridium complex **IrBNacac**.

DFT calculation

DFT method was used to optimize the geometries all the complexes. The electronic transition energies and electron correlation effects were also calculated by (TD)-DFT method with the B3LYP functional (TD-B3LYP). The LANL2DZ basis set was used to treat with the iridium atom, and the 6–31G(d) basis set was used to treat with all other atoms. All calculations were carried out according to the Gaussian 09 program.[2]

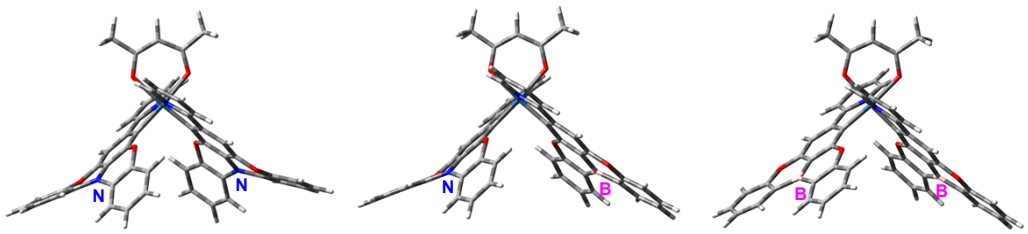

IrNNacac — **Dipole moment: 2.7972 D**

IrBNacac — **Dipole moment: 3.6306 D**

IrBBacac — **Dipole moment: 4.1213 D**

Figure S7. Optimized structures and dipole moment for **IrNNacac**, **IrBNacac** and **IrBBacac** at the ground state (S_0).

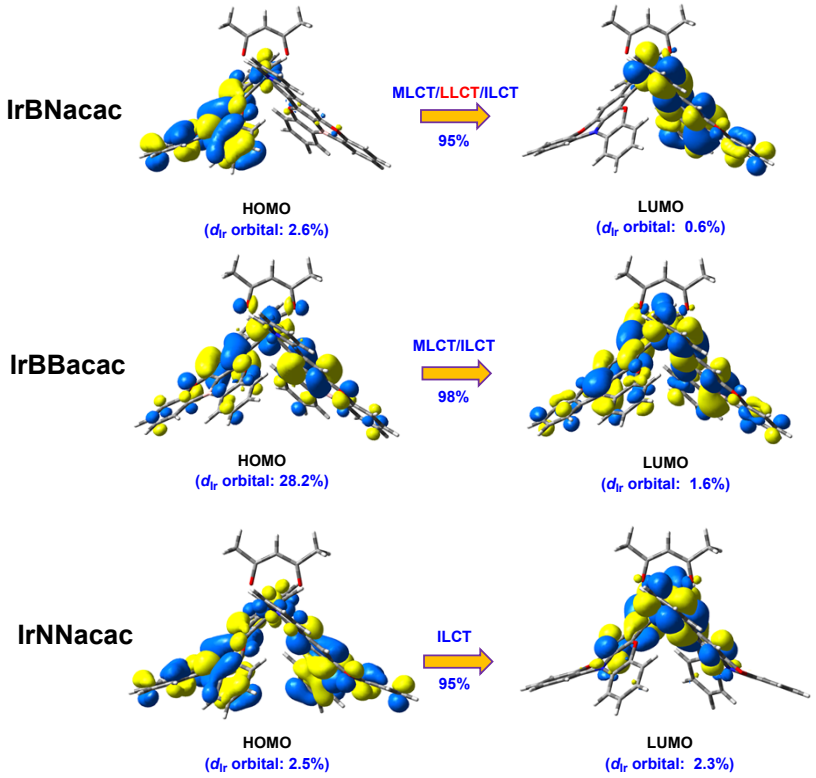

Figure S8. The orbital distribution for all the iridium complexes at the S_1 state.

Table S4. Calculated energies and oscillator strengths for lowest-energy singlet (S_1) and triplet (T_1) transitions.

Complexes	states	E (eV)	Oscillator strength	main configurations (CI coeff)	Character
IrBNacac	S_1	2.2791	0.0081	HOMO→LUMO (0.95)	MLCT/LLCT/ ILCT
	T_1	1.6327	0	HOMO-1→LUMO (0.58)	^{3}MLCT/^{3}LLCT/^{3}ILCT
				HOMO→LUMO (0.37)	^{3}MLCT/^{3}LLCT/^{3}ILCT
IrBBacac	S_1	2.2299	0.0001	HOMO→LUMO (0.98)	MLCT/ILCT
	T_1	1.6023	0	HOMO→LUMO (0.90)	^{3}MLCT/^{3}ILCT
IrNNacac	S_1	2.5890	0.0439	HOMO→LUMO (0.95)	ILCT
	T_1	1.7132	0	HOMO→LUMO (0.90)	^{3}ILCT

OLED Device characterization

Device fabrication: The ITO-coated glass substrates with a sheet resistance of 15 Ω square^{-1} were ultrasonicated sequentially in acetone and ethanol, followed by the treatment in a UV-ozone oven for 10 min. Afterwards, PEDOT:PSS (CLEVIOS P VP AI 4083) was spin-coated onto the ITO substrates at ambient temperature at a speed of 4000 rpm for 40 s (~35 nm). The PEDOT:PSS-coated ITO substrates were then transferred to a glove box with N_2 atmosphere and baked at 120 °C for 10 min. The emissive layer (using chlorobenzene as the solvent, 10 mg/mL) was spin-coated onto the PEDOT:PSS layer at a speed of 1000 rpm for 30 s (~50 nm), followed by an annealing process (80 ^{o}C for 10 min). Then, the electron-transporting layer (TPBI, 35 nm) were deposited at a rate of ~ 2 Å/s, electron injecting layer (Liq, 2 nm) at ~ 0.2 Å/s, and cathode (aluminum, 100 nm) at ~ 4 Å/s in a vacuum chamber under 2 × 10^{-6} mbar. The thickness of the spin-coated films were measured by KLA Alpha-Step D-300. The thickness of the deposited films were monitored by an INFICON SQC-310C deposition controller. The devices were tested in ambient environment without encapsulation. The current density-voltage-luminance (*J*-*V*-*L*), *L*-*EQE* curves, and electroluminescence spectra were measured using a Keithley 2400 source meter coupled with an absolute EQE measurement system (C9920-12, Hamamatsu Photonics, Japan).

Table S5. EL performances of the device for **IrBNacac**.

Complex	V_{on}[a]	$EQE_{max}/CE_{max}/PE_{max}$[b]	λ_{ems}[c]	**CIE**[d]
	[V]	**[%/cd A^{-1}/lm W^{-1}]**	**[nm]**	**(x, y)**
IrBNacac	3.9	4.9/5.5/3.1	625	(0.64, 0.35)

[a] Voltage in the luminance of 10 cd/m^2. [b] Maximum external quantum efficiency (EQE_{max}), maximum current efficiency (CE_{max}), maximum power efficiency (PE_{max}). [c] Maximum emission wavelength of the EL spectra. [d] The Commission Internationale de l'Eclairage (CIE) coordinates.

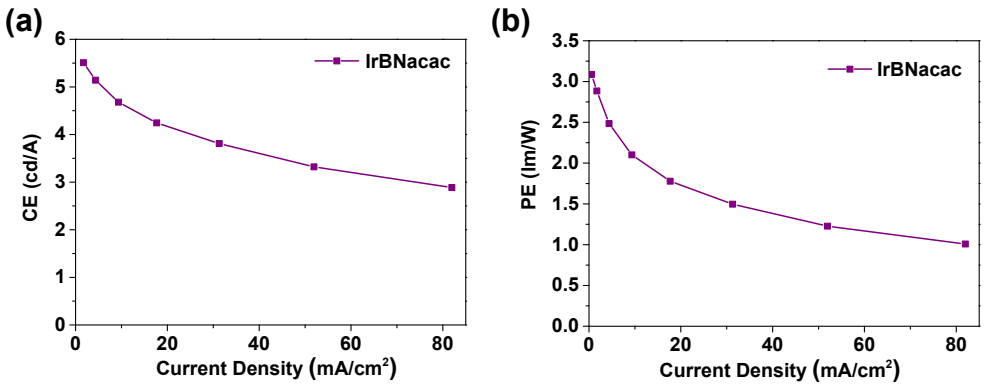

Figure S9. (a) The current efficiency and (b) powder efficiency for device of **IrBNacac**.

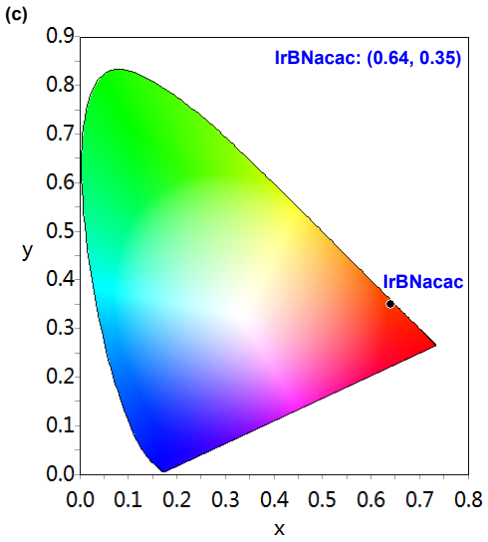

Figure S10. The CIE coordinates of electroluminescence spectra of the complex **IrBNacac** in OLED.

TG analysis

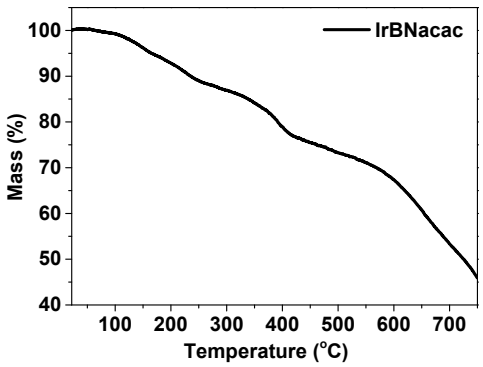

Figure S11. The TG thermograms of the complex **IrBNacac**.

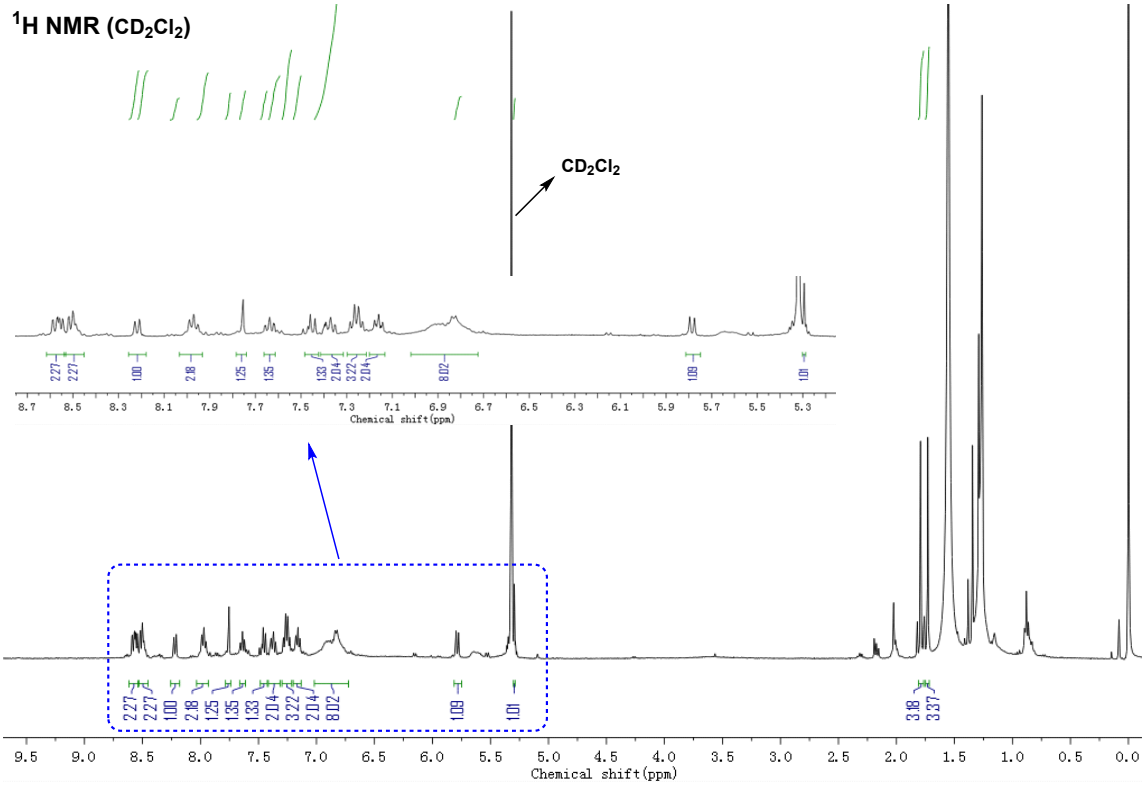

Figure S13. The ^{1}H NMR spectra of the complex **IrBNacac**.

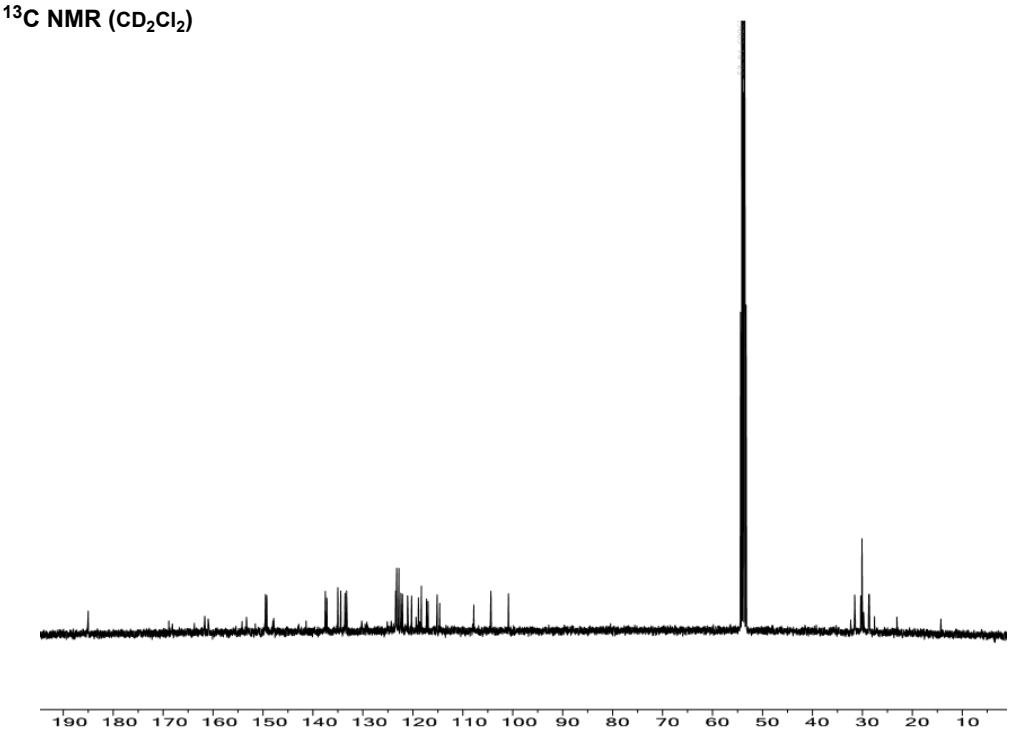

Figure S14. The ^{13}C NMR spectra of the complex **IrBNacac**.

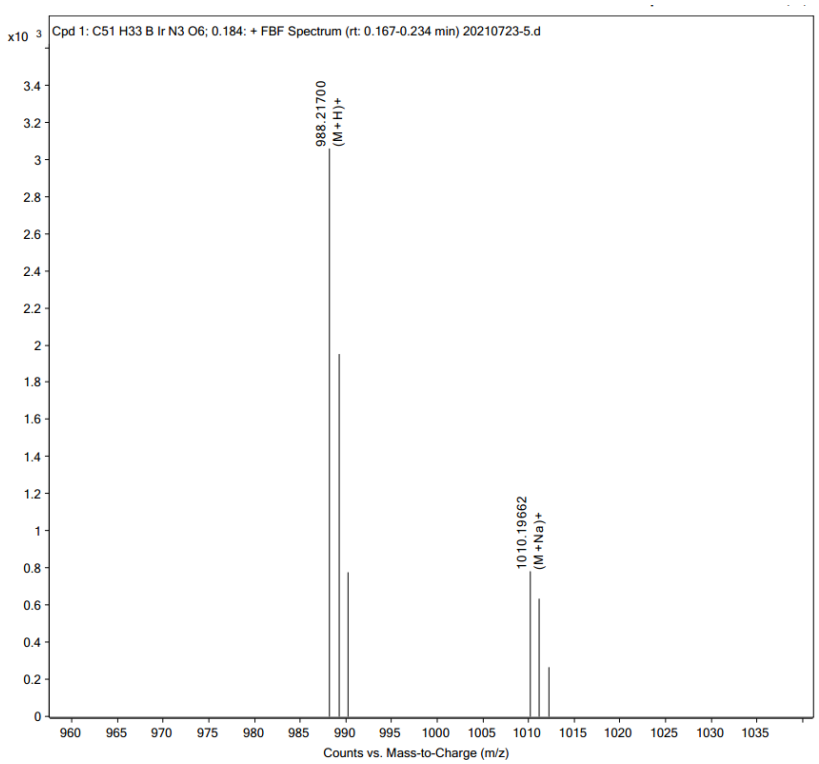

Figure S15. The high resolution mass spectrum (HRMS) of the complex **IrBNacac**.

References

1. Q. Li, C. Shi, M. Huang, X. Wei, H. Yan, C. Yang, A. Yuan, B- and N-embedded color-tunable phosphorescent iridium complexes and B–N Lewis adducts with intriguing structural and optical changes. *Chem. Sci.* **2019**, 10, 3257–3263.
2. M. J. Frisch, G. W. Trucks, H. B. Schlegel, G. E. Scuseria, M. A. Robb, J. R. Cheeseman, G. Scalmani, V. Barone, B. Mennucci, G. A. Petersson, H. Nakatsuji, M. Caricato, X. Li, H. P. Hratchian, A. F. Izmaylov, J. Bloino, G. Zheng, J. L. Sonnenberg, M. Hada, M. Ehara, K. Toyota, R. Fukuda, J. Hasegawa, M. Ishida, T. Nakajima, Y. Honda, O. Kitao, H. Nakai, T. Vreven, J. A. Montgomery Jr., J. E. Peralta, F. Ogliaro, M. Bearpark, J. J. Heyd, E. Brothers, K. N. Kudin, V. N. Staroverov, T. Keith, R. Kobayashi, J. Normand, K. Raghavachari, A. Rendell, J. C. Burant, S. S. Iyengar, J. Tomasi, M. Cossi, N. Rega, J. M. Millam, M. Klene, J. E. Knox, J. B. Cross, V.Bakken, C. Adamo, J. Jaram illo, R. Gomperts, R. E. Stratmann, O. Yazyev, A. J. Austin, R. Cammi, C. Pomelli, J. W. Ochterski, R. L. Martin, K. Morokuma, V. G. Zakrzewski, G. A. Voth, P. Salvador, J. J. Dannenberg, S. Dapprich, A. D. Daniels, O. Farkas, J. B. Foresman, J. V. Ortiz, J. Cioslowski and D. J. Fox, Gaussian 09, Revision B.01, Gaussian, Inc., Wallingford CT, **2010**.